



1 **Dominant Influence of Biomass Combustion and Cross-Border Transport on Nitrogen-Containing Organic**
2 **Compound Levels in the Southeastern Tibetan Plateau**

3

4 Meng Wang^{1,2}, Qiyuan Wang^{1,3,*}, Steven Sai Hang Ho⁴, Jie Tian¹, Yong Zhang¹, Shun-cheng Lee^{5,*}, Junji Cao⁶,
5 *

6 ¹State Key Laboratory of Loess and Quaternary Geology, Institute of Earth Environment, Chinese Academy of
7 Sciences, Xi'an 710061, China

8 ²Department of Civil and Environmental Engineering, The Hong Kong Polytechnic University, Hung Hom, Hong
9 Kong

10 ³CAS Center for Excellence in Quaternary Science and Global Change, Xi'an 710061, China

11 ⁴Division of Atmospheric Sciences, Desert Research Institute, Reno, NV89512, United States

12 ⁵Function Hub, Thrust of Earth, Ocean and Atmospheric Sciences, The Hong Kong University of Science and
13 Technology (Guangzhou), 511400 Guangzhou, China

14 ⁶Institute of Atmospheric Physics, Chinese Academy of Sciences, Beijing 100029, China

15

16 *Correspondence to:* Qiyuan Wang (wangqy@ieecas.cn), Shun-cheng Lee (shunchenglee@hkust-gz.edu.cn), and
17 Junji Cao (jjcao@mail.iap.ac.cn)



18 **Abstract**

19 The Tibetan Plateau (TP) is highly susceptible to climate change and the nitrogen-containing organic compounds
20 (NOCs) in fine particulate matter (PM_{2.5}) represent one of the large uncertainties in affecting the climate in high-
21 altitude areas. Previous studies have shown that NOCs play a vital role in the nitrogen budget of PM_{2.5}. However,
22 our understanding of the composition and sources of NOCs in PM_{2.5}, particularly in TP, is limited. Here, we aim
23 to enhance our understanding of NOCs in the TP region by examining their identification, concentration levels,
24 sources, and origins. We conducted field sampling at a regional background sampling site in Gaomeigu, in the
25 southeastern margin of TP from March 11th to May 13th in 2017. The daily mass concentrations of NOCs ranged
26 from 714.4 to 3887.1 ng m⁻³, with an average of (2119.4 ± 875.0 ng m⁻³) during the campaign. This average
27 concentration was approximately 40% higher than that reported at a typical regional site in the North China Plain
28 (NCP), highlighting a more significant presence of NOCs in the Tibetan area. Biomass burning and secondary
29 sources were identified as the major contributors to total NOCs. This was further substantiated by a regional air
30 quality model, which indicated that over 80% of the aerosol in the southeast of TP originated from neighboring
31 countries. This study enhances our understanding of NOCs' contribution to PM_{2.5} in TP and their potential impacts
32 on the climate stability in high-altitude areas.

33

34 **Keywords:** Southeastern Tibetan Plateau, Nitrogen-containing organic compounds, Source apportionment,
35 Receptor model,

36



37 **1 Introduction**

38 The Tibetan Plateau (TP), located near densely populated and industrialized regions, is particularly susceptible to
39 climate change (Meng et al., 2013; Duo et al., 2015; Li et al., 2015; Yuan et al., 2016; Zhao et al., 2022). The
40 dry season features prevalent natural forest fires and anthropogenic burning activities, such as the combustion of
41 agricultural residues, leading to substantial emissions of atmospheric pollutants (Zhao et al., 2015; Ran et al.,
42 2022; Arun et al., 2021). Consequently, aerosol concentrations in the TP, especially during the premonsoon period,
43 have risen markedly (Han et al., 2020). Previous studies in the Tibetan region have mainly focused on
44 carbonaceous organic aerosols (OA), with nitrogen-containing organic compounds (NOCs) garnering less focus
45 (Zhang et al., 2020; Zhang et al., 2019; Chen et al., 2014). NOCs play an important role in modulating climate,
46 primarily through their light absorption abilities which influence aerosol radiative effects (Li et al., 2023). These
47 compounds actively contribute to the formation of new particulate matter and secondary organic aerosols (SOAs),
48 affecting cloud properties and the Earth's energy balance (Lin et al., 2021; Yu et al., 2024). The anthropogenic
49 augmentation of nitrogen emissions has notably disrupted the global nitrogen cycle, with NOC deposition
50 emerging as a significant source of reactive nitrogen (Li et al., 2023). This has profound implications for
51 atmospheric chemistry and climate, necessitating a deeper understanding of NOC sources and atmospheric
52 processes in the climate-sensitive region of TP.

53 The pre-monsoon period features meteorological conditions that facilitate the long-range transport of NOC-
54 containing aerosols onto the TP, with prevailing atmospheric circulations transporting pollutants from neighboring
55 countries in southwest China (Wang et al., 2019a). Anthropogenic biomass burning is more intensive during the
56 pre-monsoon period and the incoming NOCs associated with biomass burning may have the potential to alter the
57 chemical composition of the atmosphere, influence cloud microphysics, and affect the regional radiative balance
58 during a critical time of hydrological accumulation and ecological transition (Tan et al., 2021). Given the TP's
59 significance in the Asian water cycle and its role as a global climate regulator, the poorly characterized
60 atmospheric behavior of NOCs during the pre-monsoon season represents a significant knowledge gap (Li et al.,
61 2023).

62 Over the past decade, studies on NOCs have primarily focused on identifying their sources and concentrations
63 (Song et al., 2017; Boreson et al., 2004; Barbaro et al., 2015; Lin et al., 2021). More than 200 NOCs have been
64 detected in the atmosphere, originating from a variety of natural sources such as animals, vegetation, ocean, and
65 husbandry, as well as anthropogenic sources including sewage treatment, combustion processes, vehicle emissions,
66 and industrial activities (Zhu et al., 2020; Zhang and Anastasio, 2003b; Shi et al., 2010; Ho et al., 2019; Wang et
67 al., 2022). Determining the sources of NOCs in the atmosphere remains challenging. For example, studies have
68 identified the sources of specific NOCs like amines, amino acids, amides, nitriles, urea, and nitrophenol (Ge et
69 al., 2011). Notably, Amines are prevalent in both urban and rural areas in America, mainly derived from industrial
70 and animal husbandry (Sorooshian et al., 2008). Biomass burning and animal farming are known emission
71 pathways for amino acids (Zhang and Anastasio, 2003a). Furthermore, investigations have shown that a
72 significant portion of water-soluble organic nitrogen (WSON) may form secondarily, as indicated by its
73 correlations with water-soluble ionic species like nitrate (NO_3^-), sulfate (SO_4^{2-}), and ammonia (NH_4^+) (Ho et al.,
74 2015). Amides can react with atmospheric acidic particles, forming secondary aerosols (Priestley et al., 2018).
75 Although previous studies have focused on identifying sources of prevalent NOCs (e.g., amino acids and amines)
76 via tracer correlations, uncertainties about specific NOC concentrations and their sources persist. Recent studies
77 have employed receptor models for source apportionment (Yu et al., 2024), yet a comprehensive understanding
78 of NOCs is still lacking.

79 In this study, we collected fine particulate matter ($\text{PM}_{2.5}$) samples during the pre-monsoon season at a high-
80 altitude, remote location near the Sino-Burmese border along the southeastern edge of the TP. The collected



81 samples were analyzed to determine their NOCs as well as carbonaceous components, water-soluble ions, and
82 elements. The objectives of the study were to investigate the general attributes and chemical composition of NOCs,
83 ascertain the contribution of various sources to these compounds, and identify the source regions influencing
84 PM_{2.5} and specific chemical constituents in the area.

85 **2 Experimental**

86 **2.1 Sampling**

87 Aerosol sampling was conducted at the Lijiang Astronomical Station, the Chinese Academy of Sciences
88 (26.70°N, 100.03°E, 3260 m above the sea level, Fig. S1) in Gaomeigu from March 11th to May 13th 2018. The
89 location is approximately 2 km away from the Gaomeigu village and 30 km from Lijiang City, located on the
90 southeastern edge of the TP (Zhao et al., 2019; Wang et al., 2019a). The surrounding area comprises farmland
91 and forests, with no obvious industrial proximity. Two highways are situated about 6 km from the sampling site.
92 Daily PM_{2.5} samples were collected using a high-volume sampler (model TE-6070 Tisch Inc., Village of Cleves,
93 OH, USA) at a flow rate of 1.13 m³ min⁻¹. The aerosol samples were collected on quartz fiber filters (20.3 cm ×
94 25.4 cm, Whatman QM/A, Clifton, NJ, USA) that had been pre-heated to 780 °C for 3 h for removing
95 carbonaceous materials. The sampling equipment was positioned approximately 10 m above the ground level on
96 a building's rooftop. All sampled filters were enveloped in clean aluminum foils and stored at -20 °C in a freezer
97 until subsequent analysis in the laboratory. To account for background levels, field blank filters were processed
98 and analyzed as the same method as the PM samples. All data presented was subtracted by field blank values.

99 **2.2 NOCs analysis**

100 A total of 64 PM_{2.5} samples were analyzed to determine the target NOCs in this study. Amines and amino acids
101 were quantified with the derivatization and analytical procedures by the Waters' AccQ-Tag method (Cohen and
102 Michaud, 1993; Ho et al., 2015; Ho et al., 2019). For sample extraction, a 4.3 cm² filter was cut into pieces and
103 subjected to ultrasonic extraction with 5 mL of Milli-Q water (18 MΩ cm) twice in a water bath at 25 °C. Each
104 extract was then filtered through a 0.45 μm filter and concentrated to 0.5 mL using a rotary evaporator under
105 vacuum. The resulting extracts were reacted with 6-aminoquinolyl-N-hydroxysuccinimidyl carbamate (AQC) to
106 produce fluorescent derivatives. The AccQ-Fluor reagent kit (WAT052880, Waters Corporation, Milford, MA,
107 USA) consists of AQC and AccQ. Tag borate buffer, and AccQ. Tag Eluent A was used for the derivatization
108 process. The derivatized sample extracts were reconstituted and stored in a desiccator at room temperature before
109 analysis. In the HPLC analysis, the derivates and calibration standards were injected into the high-performance
110 liquid chromatography (HPLC, 1200 Series, Agilent Technology, Santa Clara, CA, USA) equipped with a
111 fluorescence detector. The sample vials were heated at 55 °C for 10 minutes using the oven within the system.
112 The mixture was separated using a column (3.9 × 150 mm AccQ.Tag Amino Acid Analysis Silica base) bonded
113 with a 4-μm C-18 reversed-phase column at 37 °C and detected at an absorption wavelength of 395 nm. The
114 linearity of the calibrations was assessed by the correlation coefficient ($R^2 > 0.999$), and the minimum detection
115 limits (MDLs) for the target organic nitrogen species ranged from 0.036 to 0.086 nmol m⁻³. To ensure the
116 reliability of the analysis, one replicate analysis of the ambient sample was conducted for every 10 samples.
117 Additionally, ambient samples spiked with known amounts of internal and external standards were analyzed to
118 assess potential interference from the sample matrix.

119 For alkyl amides, alkyl nitriles, isocyanates, and cyclic NOCs, the extraction procedures were the same as those
120 used for the FAAs. After extraction, combination, filtration, and concentration, the extracts were mixed with 50



121 μL of borate buffer to adjust the pH to 9.1. The solutions were then diluted with a water/acetone mixture (3:1, v/v)
122 to a final volume of 150 mL. To this mixture, 40 mL of dansyl chloride in acetone and 10 mL of an internal
123 standard were added. The resulting mixture underwent a derivatization reaction, which involved vortex agitation
124 for 1 minute and subsequent ultrasound irradiation at 35 °C for 15 minutes, following the method described by
125 Ruiz-Jiménez et al. (2012). The reaction vials were kept in the dark until the analysis. The derivatized products
126 were introduced into the HPLC system, which was equipped with a 2.1 \times 150 mm C18 column (3.5- μm particle
127 size, Waters Sunfire), and coupled with an ion-trap mass spectrometer (Esquire 3000, Bruker Daltonics). The
128 linearity of the calibrations for these compounds was evaluated using the correlation coefficient ($R^2 > 0.999$). The
129 MDL for the target organic nitrogen species ranged from 0.005 to 0.019 nmol m^{-3} .

130 Urea was identified and quantified using a direct injection method on an HPLC system coupled with a
131 photodiode array detector (DAD) (1200 Series, Agilent Technology). The separation of urea was achieved using
132 a 4.6 \times 150 mm C18 column (4- μm particle size, Cogent Bidentate), and its detection was performed at an
133 absorption wavelength of 210 nm (Ho et al., 2019). The calibration of the method exhibited a high correlation
134 coefficient ($R^2 > 0.999$), indicating a strong linear relationship between the concentration of urea and the detector
135 response. The MDL for urea was determined to be 0.05 ng mL^{-1} , denoting the lowest concentration of urea that
136 could be reliably detected using the analytical method. By employing this direct injection approach, along with
137 the specific column and detection parameters, accurate identification and quantification of urea in the samples
138 were achieved. The high linearity of the calibration and low MDL underscore the sensitivity and reliability of the
139 method for analyzing urea content in the study.

140 2.3 Auxiliary measurements

141 Organic carbon (OC), elemental carbon (EC), organic markers including polycyclic aromatic hydrocarbons (PAHs)
142 and levoglucosan, and elemental components of $\text{PM}_{2.5}$ including Ca, Ti, V, Mn, Fe, Cu, As, Br, Pb, and Zn were
143 also determined (Table S1). Further details regarding the chemical analyses, including processes, accuracies,
144 precisions, and quality assurance/quality control (QA/QC) procedures of auxiliary data, can be found in Text S1
145 in Supplement Information.

146 2.4 Estimation of secondary organic carbon (SOC)

147 In this study, an approach called the minimum R^2 (MRS) method was utilized to estimate [SOC] concentration
148 (Wu and Yu, 2016) which is deduced using the following equations:

$$149 \quad [\text{SOC}] = [\text{OC}] - [\text{POC}] \quad (1)$$

$$150 \quad [\text{POC}] = [\text{EC}] \times (\text{OC/EC})_{\text{primary}} \quad (2)$$

151 where [OC] and [EC] represent the measured concentrations, [POC] represents the primary organic carbon
152 concentrations, and $(\text{OC/EC})_{\text{primary}}$ denotes an estimate of the primary OC/EC ratio. We calculated a series of
153 $(\text{OC/EC})_{\text{primary}}$ values to achieve the lowest coefficient of determination (R^2) between [SOC] and [EC], as shown
154 in Fig. S2. This minimization of R^2 allows the accurate deduction of SOC levels, considering the relationship
155 between [SOC] and [EC].

156

157 2.5 Source apportionment

158 Source apportionment using Positive Matrix Factorization (PMF) with the multilinear engine (ME-2) was
159 performed by employing the source finder tool SoFi v6.7 (Canonaco et al., 2013). The analysis involved aligning
160 daily measurements of seven nitrogen organic classes with concurrent measurements of three carbonaceous



161 materials (EC, POC, and SOC), one water-soluble inorganic ion (K^+), and 10 elements (Ca, Ti, V, Mn, Fe, Cu,
162 As, Br, Pb, and Zn) in the $PM_{2.5}$ fraction. The characteristics of the input species and the correlation matrix of
163 each species can be found in Table S2 and Fig. S3, respectively, providing statistical information for the analysis.
164 Details of the PMF and ME-2 analysis can be found in the supplementary (Text S1). Briefly, we first performed
165 unconstrained PMF with a factor number of 2-12 and examined the factor profile and time series (Fig. S4-7). 7-
166 factor factors were determined as the optimum solution (Fig. S8 and S9). To reduce the mixing between the factors,
167 a constrained PMF analysis using the “a value” approach of the ME-2 solver was applied (Canonaco et al., 2013).
168 The 7-factor with the constrained matrix is shown in Table S2. The constrained run was performed by adding
169 constraints in the base run resolved factor profiles so that the tracers are only present in the corresponding sources
170 (Wang et al., 2019b).

171

172 **2.6 Potential source contribution function (PSCF)**

173 The potential source contribution function (PSCF) was used to identify the likely pollution regions that influenced
174 PMF factors based on back trajectories. PSCF analysis was performed using Zefir (Petit et al., 2017). Each
175 trajectory includes a range of latitude–longitude coordinates every 1-hr backward in a whole day. The studying
176 field is from 20 to 30 °N, and 90 to 105 °E, which includes more than 95% of the area covered by all the paths.
177 The set of trajectory data for each arriving elevation level contained two trajectories per day. More details of the
178 PSCF analysis can be found in Text S1.

179

180 **2.7 Community Multiscale Air Quality**

181 The Community Multiscale Air Quality (CMAQ) model (Version 5.4) was applied to assess the transport of
182 aerosols from neighboring countries in southwest China. The CMAQ model was configured with the aero7 aerosol
183 module and cb6r5 gas-phase mechanism (Murphy et al., 2021). The model adopted a horizontal grid resolution
184 of 27 km, consisting of 34 vertical layers.

185 To generate the necessary meteorological fields for the CMAQ simulations, the Weather Research and
186 Forecasting (WRF) model (version 4.4) was utilized. The initial and boundary conditions for WRF were obtained
187 from the National Centers for Environmental Prediction (NCEP) Final (FNL) dataset, which is a reanalysis dataset.
188 For the domestic emission inventory, the Multiresolution Emission Inventory for China (MEIC) was employed.
189 Additionally, the MIX inventory was used to account for emissions from other countries (Li et al., 2017).

190 Two simulation cases were conducted: one considering only domestic emissions (i.e., MEIC), and the other
191 considering emissions from both domestic and other countries (i.e., MEIC + MIX). By employing the zero-out
192 method, the differences between these two cases represented the contribution of emissions from other countries
193 to the $PM_{2.5}$ levels in the study area. The CMAQ simulations were performed from March 9th to March 27th, 2018,
194 with the first 3 days considered a spin-up period for the model. The simulation period covered the first two weeks
195 of the campaign, encompassing the period before and during the initial pollution event from March 22nd to March
196 26th. CMAQ reproduced the measured $PM_{2.5}$ at GMG reasonably well when considering both MEIC and MIX in
197 the emission inventory, with a correlation coefficient of $r > 0.9$ between the modeled and measured $PM_{2.5}$ and a
198 slope of 0.61 (Fig. S11).



199 **3 Results and discussion**

200 **3.1 Overview of NOC Concentration**

201 Figure 1 illustrates the concentration variations of NOCs, carbonaceous aerosols, and meteorological parameters
202 in Gaomeigu during the campaign. The daily mass concentrations of NOCs range from 714.4 to 3887.1 ng m⁻³,
203 with an average of 2119.4 ± 875.0 ng m⁻³. This average is approximately 40% greater than the NOCs concentration
204 observed at a regional site in Xianghe, China (1270 ng m⁻³) (Wang et al., 2022). The NOCs are classified into
205 major (> 10% contribution) and minor (< 10% contribution) compounds, as detailed in Table 1, with the major
206 classes including FAAs, amines, and urea. The average concentrations of these major NOCs are 1922.6 ± 790.5
207 ng m⁻³, dominated by FAAs (58.9%), followed by amines (28.0%), and urea (13.7%). Minor NOC species such
208 as alkyl amides, alkyl nitriles, isocyanates, and cyclic NOCs have average concentrations of 45.1 ± 18.6 ng m⁻³,
209 4.68 ± 1.75 ng m⁻³, 10.9 ± 4.73 ng m⁻³, and 136.2 ± 61.6 ng m⁻³, respectively.

210 As shown in Fig. 1, the campaign is segmented into five periods (EC1-EC5) based on meteorological conditions
211 and NOC concentration variations. The clean period featured a temperature consistently above 9 °C and an
212 average OC concentration of 2137.3 ± 296.7 ng m⁻³. Elevated wind speeds during this period (4.4 ± 1.3 m s⁻¹)
213 enhanced atmospheric dispersion relative to other polluted periods. Notably, average NOC concentration
214 increased during high NOC concentration periods, reaching 1482.6 ± 346.4 ng m⁻³, which is more than triple the
215 level observed during the clean period (451.8 ± 65.2 ng m⁻³). Delving into the high NOC concentration periods
216 individually, EP1 shows the highest aggregate concentration of major NOCs, which is 4.3 to 5.0 times greater
217 than during the clean period. The NOCs/POC ratios were 0.773 (EP1), 0.774 (EP2), 0.674 (EP3), and 0.638 (EP4),
218 presenting a stark contrast to the clean period's ratio of 0.503. However, the NOCs/SOC ratio remains relatively
219 stable across the phases. These trends underscore the significant influence of primary sources during elevated
220 NOC concentration periods. Conversely, during the clean period, the source of NOCs appears more complex,
221 suggesting a nuanced interplay of primary and secondary sources. A more in-depth discussions on source
222 apportionment are provided in Section 3.4.

223 **3.2 Major NOC Classes**

224 **3.2.1 Free Amino acids (FAAs)**

225 During the sampling campaign, the average FFA concentration is 1092.9 ± 443.37 ng m⁻³, in a range of 370.2 and
226 2033.2 ng m⁻³ (Table 1). This level is comparable with FAAs observed in regions such as rural Guangzhou, China
227 (Song et al., 2017), Arizona, U.S. (Boreson et al., 2004), and Antarctica's MZ Station, U.S. (Barbaro et al.,
228 2015) but is higher than in urban/suburban and marine regions like Nanchan, China (Zhu et al., 2020), California,
229 U.S. (Zhang and Anastasio, 2003b), Qingdao, China (Shi et al., 2010), Hong Kong, China (Ho et al., 2019).
230 Notably, the average FAAs concentration in this study is approximately four times higher than that reported in
231 Xianghe, China (Wang et al., 2022).

232 FAAs are classified into protein-type and non-protein-type categories. Table S3 provides an overview of
233 protein-type and non-protein-type FAAs, with mean concentrations of 989.5 ± 403.54 ng m⁻³ and 103.3 ± 41.76
234 ng m⁻³, respectively. Protein-type FAAs, including Asp, Ser, Glu, Gly, His, Thr, Ala, Pro, Cys, Tyr, Val, Met,
235 Lys, Ile, Leu, and Phe, accounts for 90.5% of total FAAs, with Glycine (Gly) being the most prevalent. These
236 findings are consistent with previous studies that identified Gly as the predominant FAA in Nanchang (Zhu et al.,
237 2020), Hong Kong (Ho et al., 2019), and Venice (Barbaro et al., 2011). Non-protein-type FAAs such as β-
238 alanine (β-Ala), γ-aminobutyric acid (γ-Ala), and ornithine (Orn) also contributed, with β-Ala representing 9.5%
239 of these FAAs.



240 Figure 2 illustrates a positive correlation between FAAs and O_x ($NO_2 + O_3$), indicating an association with
241 secondary formation processes post-precursor emissions. The average FAA concentration is 900 ng m^{-3} at O_x
242 levels below 70 ppb but rises above 1200 ng m^{-3} when O_x exceeds 85 ppb. Moreover, FAAs correlate strongly
243 with both POC ($r = 0.95$) and SOC ($r = 0.90$), indicating that secondary processes likely influence the FAA
244 formation, despite no obvious direct local emission near the sampling site. This suggests contributions from both
245 primary and secondary sources to the FAA levels observed.

246 Moreover, Gly comprises 31% of total FAAs and shows a similar positive relationship with O_x . The Gly
247 concentration increases from 250 ng m^{-3} when the O_x is below 70 ppb to 400 ng m^{-3} when the O_x is above 85 ppb.
248 Its correlations with POC ($r = 0.94$) and SOC ($r = 0.89$) reinforce the impact of secondary formation processes,
249 similar to patterns observed in the North China Plain (NCP) region, China (Wang et al., 2022).

250 3.2.2 Amines and urea

251 The average concentration of amines during the sampling period is 563 ng m^{-3} . Aliphatic amines dominate,
252 contributing 90% of the total amine, while aromatic amines constitute less than 1% (Fig. 3). The remaining 9%
253 includes other amine compounds including ethanolamine, galactosamine, 2-amino-1-butanol, and N-
254 methylformamide. During the pollution episodes, aliphatic amine concentrations exceed 600 ng m^{-3} , with a
255 maximum of 1000 ng m^{-3} . In contrast, during clean periods, these levels declined to $\sim 200 \text{ ng m}^{-3}$. The proportions
256 of aliphatic amines during pollution episodes are 90-91%, which decreases to 84% during clean periods, with an
257 increase in other concentrations.

258 Methylamine (MA) emerges as the predominant aliphatic amine, constituting 62% of the total aliphatic amines.
259 Ethylamine (EA) follows, contributing 28% to the total aliphatic amines. Dimethylamine (DMA), trimethylamine
260 (TMA), and other amine species together account for the remaining 10%. Both MA and EA exhibit negative
261 correlations with ambient temperature (Fig. 3), indicating the potential influence of temperature on gas-to-particle
262 partitioning. Below 12°C , the average MA concentration is around 400 ng m^{-3} , which halves to 200 ng m^{-3} as
263 temperature increases above 18°C . Similarly, EA concentration is higher at lower ambient temperatures, around
264 195 ng m^{-3} below 12°C , decreasing to 100 ng m^{-3} above 18°C . Given their low molecular weight, MA and EA are
265 more prevalent in the gas phase at elevated ambient temperatures, where they also exhibit enhanced atmospheric
266 reactivity with acids, transforming into other compounds.

267 Both MA and EA show negative correlations with RH, with elevated concentrations at lower RHs (Fig. 3d).
268 This inverse relationship might be counterintuitive, given that higher RH typically promotes the partitioning of
269 low molecular weight amine into the particle phase. However, MA and EA, being atmospheric reactive amines,
270 are involved in in-particle reactions. Under high RH conditions, increased condensation of acids and/or reactive
271 organic compounds occur, which subsequently react with MA and EA, consuming them and thus establishing a
272 negative correlation with RH.

273 Urea is identified as the third major NOC species, with an average concentration of 266 ng m^{-3} during the
274 campaign. This value is approximately half that reported at a regional site in the NCP (Wang et al., 2022), though
275 the direct comparison is limited due to spatial and temporal differences. The urea level at this elevated site
276 highlights the notable role of agricultural fertilizers as a potential source. Urea can be released into the atmosphere
277 through agricultural activities and biomass burning, and it can also be formed secondarily in the atmosphere
278 through chemical reactions.



279 **3.3 Minor NOC Classes**

280 **3.3.1 Alkyl amides and nitriles**

281 In this study, the distributions and sources of alkyl amides in a range of C₆-C₂₀ were determined in Gaomeigu.
282 Figure S10 illustrates the distribution patterns of these species during the campaign, where the concentrations of
283 n-alkyl amides vary from 1.11 to 7.57 ng m⁻³, reflecting diverse emission sources. These amides can originate
284 from anthropogenic activities such as coal combustion and vehicular traffic, as well as biogenic processes. To
285 distinguish between these sources, we use the carbon preference index (CPI) and the oleamide to stearamide ratio
286 (Cheng et al., 2006). The CPI, calculated as the ratio of the sum of odd-numbered C₇-C₁₉ alkyl amides to even-
287 numbered C₆-20 alkyl amides, helps identify the dominant source: a CPI ≤ 1 indicates anthropogenic dominance,
288 whereas > 1 suggests biogenic predominance (Abas and Simoneit, 1996). The results show that the CPI of alkyl
289 amides ranges from 0.46 to 0.75, with an average of 0.61 ± 0.05, emphasizing the anthropogenic impact on their
290 concentrations. Notably, the CPI values do not vary between the periods having low and high NOC concentrations,
291 suggesting consistent alkyl amide sources throughout the campaign, potentially influenced by long-range transport
292 and stable meteorological conditions.

293 Beyond the CPI, the R₁₈, which is a ratio of oleamide (C_{18:1}) and stearamide (C_{18:0}), serves as an indicator for
294 alkyl amide aging (Wang et al., 2022). This ratio provides insights into the precursor composition, oxidation
295 degradation, and transport processes influencing unsaturated amide concentrations (Nielsen et al., 2012). An R₁₈
296 < 1 implies the aging of alkyl amides due to long-range transport, whereas R₁₈ > 1 indicates local biomass-burning
297 emissions (Cheng et al., 2006). According to the results of this study, R₁₈ values range from 0.73 to 2.27,
298 suggesting the alternation between local and long-range transport.

299 During the sampling period, the average concentration of alkyl nitriles is 4.69 ± 1.75 ng m⁻³ in Gaomeigu. As
300 shown in Table S3, hexadecanenitrile (C₁₆) is the most prevalent (0.49 ng m⁻³), followed by tetradecanenitrile (C₁₄)
301 (0.45 ng m⁻³). The concentrations of the other analyzed alkyl nitriles are below 0.4 ng m⁻³. The results are constant
302 with the higher concentrations observed at the Xianghe site (Wang et al., 2022). Moreover, the CPI values for
303 alkyl nitriles were between 0.605 to 0.848, with an average of 0.702 ± 0.05, which points out the anthropogenic
304 influence on their levels. During high NOC concentration phases, the CPI values remain constant (i.e., EP1: 0.72,
305 EP2: 0.71, EP3: 0.71, and EP4: 0.72), compared to 0.75 during clean periods. This consistency implies that
306 anthropogenic sources predominantly influence alkyl nitrile concentrations regardless of the pollution levels.

307 Furthermore, it is important to note that alkyl amides and nitriles might form as secondary products during
308 biomass burning through reactions between ammonia (NH₃) and FAAs (Simoneit et al., 2003). The link between
309 biomass burning and the generation of these compounds is reinforced by robust correlations with levoglucosan
310 and K⁺ in Fig. S3 (r > 0.88, p < 0.01), both recognized as markers for biomass burning (Wang et al., 2018; Liu
311 et al., 2021b). These evidences firmly confirm that biomass burning is a key contributor to the occurrence of alkyl
312 amides and nitriles in the region.

313 **3.3.2 Cyclic NOCs and isocyanates**

314 The average mass concentration of cyclic NOCs is 136.2 ng m⁻³. This study identified five cyclic NOCs (Table
315 S3), with caprolactam being the most prevalent at 54.2 ng m⁻³ (39.8% of the total cyclic NOC), which is commonly
316 used in commercial manufacturing processes and lysine synthesis (Cheng et al., 2006). Other cyclic NOCs include
317 isoindole-1,3-dione (50.7 ng m⁻³, 37.2%), N-butyl-benzen-sulfonamide (NBBS) (22.1 ng m⁻³, 16.2%), N,N-
318 diethyl-m-toluamide (DEET) (5.79 ng m⁻³, 4.3%), and benzothiazolone (3.36 ng m⁻³, 2.5%). These compounds
319 are known to pose health risks (Cheng et al., 2006; Balducci et al., 2012), which primarily originate from



320 industrial and agricultural activities (Wang et al., 2022; Richardson and Ternes, 2018; Trapp and Eggen, 2013). In
321 comparison with the findings of the Xianghe site (Wang et al., 2022), the concentrations of cyclic NOCs in this
322 study are lower, indicating the lower contributions of industrial sources. During the four high NOC emission
323 periods, the concentrations of cyclic NOCs are 2-4 times higher than those during the clean period, suggesting the
324 influence of pollution levels.

325 Isocyanates, commonly used in polyurethane resin production, are associated with several health threats,
326 including asthma, allergies, and skin reactions (Lesage et al., 2001). The average total mass concentration of
327 eight isocyanates is $10.89 \pm 4.73 \text{ ng m}^{-3}$ (Table 1) while the individual concentration of each isocyanate is given
328 in Table S3, including methyl isocyanate (MIC), toluene-2,4-diisocyanate (2,4-TDI), toluene-2,6-diisocyanate
329 (2,6-TDI), isophorone diisocyanate (IPDI), 1,6-hexamethylene diisocyanate (1,6-HDI), ethyl isocyanate (EIC),
330 phenyl isocyanate (PHI), and propyl isocyanate (PIC). Among these, TDI and HDI are predominantly used in
331 industry (Hejna et al., 2024). TDI is commonly utilized in various foam products (Akindoyo et al., 2016), while
332 HDI is essential in polyurethane paints and coatings (Golling et al., 2019). The presence of these isocyanates in
333 numerous products is linked to heightened health hazards, such as skin allergies, atopic dermatitis, and various
334 respiratory diseases (Nawrot et al., 2008).

335 3.4 Sources apportionment of NOCs

336 In this study, a constrained PMF analysis was applied to identify the sources of NOCs, which include biomass
337 burning, coal combustion, industry-related sources, crustal sources, traffic emissions, agriculture activities, and
338 secondary sources (Fig. 4).

339 Factor 1, attributed to biomass burning, was characterized by high loadings of K^+ (84.3%) and levoglucosan
340 (100%), recognized tracers for biomass-burning activities (Liu et al., 2021a; Lin et al., 2018). This factor also has
341 a notable Zn content (38.7%), indicative of wood burning (Salam et al., 2013). Biomass burning contributes 26.3%
342 to the total NOCs, emerging as the second-largest emission category. Factor 2, associated with coal combustion,
343 exhibits substantial loadings of As and also contains Cu, Pb, and EC. As and Pb are typical tracers of coal
344 combustion (Qin et al., 2019), and Cu is also associated with coal combustion (Hsu et al., 2016). Factor 3 is
345 recognized as industry-related emissions which is characterized by high loading of cyclic NOCs and isocyanates,
346 which are synthetic compounds (Wang et al., 2022). It also exhibits a significant characteristic value of Pb, which
347 can be released during industrial processes (Wang et al., 2015). This factor accounts for 7.6% of NOCs. Factor
348 4, characterized by crustal sources, had high loadings of Ti and moderate loadings of Mn, Fe, Ca, and arabitol.
349 These elements are acknowledged as crustal constituents (Gosselin et al., 2016), and arabitol is typically released
350 from soil fungal spores (Wang et al., 2018), contributing to 6.1% of the total NOCs. Factor 5, linked to traffic
351 emissions, showed high loadings of V, Br, Zn, and Cu. V acts as an indicator for heavy oil combustion in marine
352 vessels (Bian et al., 2018), and Br is a tracer of motor vehicle emissions (Guo et al., 2009). Emissions of Zn and
353 Cu are associated with brake, tire, and road wear (Salameh et al., 2018; Liu et al., 2021a). Factor 6, named
354 agriculture activities, exhibited relatively high loading of urea and moderate loadings of K^+ , Ca, and Mn in NOCs.
355 These elements are commonly used in agriculture (Ge et al., 2011), with K^+ being crucial for plant growth and
356 metabolic functions (Meena et al., 2014), and Mn playing roles in plant oxidation-reduction (Gonçalves et al.,
357 2022). This factor accounted for a portion of NOCs. Factor 7, ascribed to secondary sources, demonstrated
358 considerable influence on the SOC (Secondary Organic Carbon) variation. It was responsible for 30.2% of the
359 NOCs, emerging as the predominant emission source, highlighting the role of secondary production in both local
360 and regional pollutant formation.

361 Figure 5 illustrates the average contributions of the seven identified sources to each NOC species and the total
362 NOC. The analysis demonstrated that secondary sources and biomass burning were predominant, together



363 constituting over 50% of total NOCs (Figure 5a). Specifically, for FAAs (Figure 5b), secondary sources (39.6%)
364 and biomass burning (37.3%) are the two major contributors, while other sources accounted for less than 10%.
365 The notable influence of secondary sources and biomass burning on FAAs could be attributed to increased
366 transportation and biomass/wildfire heating in the region, consistent with findings in a previous study (Zhang et
367 al., 2018).

368 In the context of amines, agriculture activities make a notable contribution (18.8%), twice as high as its
369 contribution to FAAs (9.3%). For alkyl amides and nitriles, secondary sources and biomass burning were the
370 primary contributors, each surpassing 30%. This contrasts with findings from another study in a different Chinese
371 region where biomass burning is predominant in these NOC categories (Wang et al., 2022). These significant
372 contributions from biomass burning and secondary sources underscore the impact of regional transportation on
373 NOC sourcing within this area.

374 **3.5 Influence from long-range transport and biomass burning in Gaomeigu**

375 Figure 6 presents the spatial distribution of PM_{2.5} concentrations during the high NOC events, analyzing
376 two scenarios: one with only domestic emissions (MEIC-China) and another incorporating both domestic
377 and foreign emissions (MEIC-China + MIX). With solely domestic emissions considered, PM_{2.5} levels at the
378 GMG and across the broader Tibet region, as well as western Sichuan and Yunnan, were relatively low, not
379 exceeding 5 $\mu\text{g m}^{-3}$ (Fig. 6a). However, incorporating international transport into the analysis revealed a
380 significant increase in PM_{2.5} levels at GMG, where daily concentrations exceeded 20 $\mu\text{g m}^{-3}$ (Fig. 6c).
381 Similarly, elevated PM_{2.5} concentrations, reaching above 40 $\mu\text{g m}^{-3}$, were observed in southeast Tibet and
382 western Sichuan and Yunnan. Figure 6b presents the relative contributions of domestic and international
383 emissions at GMG. The contribution from international transport varied from 25% to 92%, overshadowing
384 domestic sources, which did not exceed 25% for most of the time. Notably, during the high NOC event, the
385 contribution from international transport increased to over 80% for the study area (Fig. 6d).

386 The emission inventory used in this study did not include data on NOCs; hence, NOCs were not explicitly
387 simulated in the CMAQ model. However, the marked influence of international transport indicates that
388 PM_{2.5}-bound NOC species likely originated from international sources, corroborated by PSCF analysis
389 linking NOCs to specific PMF factors (Fig. S12). The contribution hotspots in India and Myanmar indicate
390 that the long-range transport of biomass-burning emissions to the study area is facilitated by prevailing winds.
391 Conversely, secondary NOC sources were predominantly linked to air masses from Myanmar, implying
392 proximate secondary formation through atmospheric reactions of precursor gases and pollutants. The
393 complex atmospheric chemistry leading to secondary NOCs includes the oxidation of precursor compounds
394 such as volatile organic compounds (VOCs) and nitrogen oxides (NO_x).

395 Similar spatial patterns were observed for factors related to coal combustion, industry-related sources,
396 crustal sources, traffic emissions, and agricultural activities. This implies that their contributions were
397 associated with the proximity of the sampling site to their respective source origins. For instance, NOCs
398 related to coal combustion were potentially transported from the nearby mining or industrial areas, while
399 industry-related sources could have originated from regional transmission or industrial activities in the
400 vicinity. Crustal sources, which involve the resuspension of dust particles, could be influenced by local soil
401 conditions and wind patterns.



402 **4 Conclusions**

403 In conclusion, this study provides valuable insights into the composition, sources, and transport of NOCs in the
404 study area. The average daily mass concentrations of NOCs during the campaign ranged from 714.4 to 3887.1 ng
405 m⁻³, with an average of 2119.4 ± 875.0 ng m⁻³. The major NOC species include free amino acids (FAAs), amines,
406 and urea, accounting for 58.9%, 28.0%, and 13.7% of the major NOCs, respectively. Minor NOC species such as
407 alkyl amides, alkyl nitriles, isocyanates, and cyclic NOCs were also identified. The PMF analysis revealed seven
408 distinct sources of PM_{2.5}, with biomass burning and secondary sources as the primary contributors to total NOCs.
409 Biomass burning sources exhibited hotspots of contribution from India and Myanmar, indicating long-range
410 transport. Secondary sources, predominantly originating from Myanmar, suggested the formation of NOCs during
411 the transport. This is confirmed by the CMAQ modeling. The study also revealed the possible aging of NOCs
412 from biomass-burning sources as they approached the measurement site, highlighting the impact of atmospheric
413 transformation processes. Contributions from industry-related sources, crustal sources, and agricultural activities
414 were influenced by both regional transmission and local emissions in the vicinity of the sampling site. Overall,
415 this research highlights the complex nature of NOCs and their sources, emphasizing the interplay between long-
416 range transport, regional emissions, atmospheric chemistry, and local influences. These findings contribute to our
417 understanding of air pollution dynamics and provide a basis for developing targeted mitigation strategies and
418 policies to reduce NOC emissions and their impacts on air quality and human health in the study area and similar
419 regions.

420

421 **Declaration of competing interest**

422 The authors declare that they have no known competing financial interests or personal relationships that could
423 have appeared to influence the work reported in this paper.

424 **Credit authorship contribution statement**

425 Meng Wang: Conceptualization, Methodology, Validation, Formal Analysis, Writing - Original Draft.

426 Qiyuan Wang: Conceptualization, Writing - Review and Editing, Funding Acquisition.

427 Steven Sai Hang Ho: Formal analysis, Writing - Review, and Editing.

428 Jie Tian: Investigation.

429 Yong Zhang: Investigation, Formal analysis.

430 Shun-cheng Lee: Resources.

431 Junji Cao: Conceptualization, Writing - Review and Editing, Funding Acquisition, Supervision.

432 **Acknowledgments**

433 This work was supported by the Second Tibetan Plateau Scientific Expedition and Research Program (STEP)
434 (2019QZKK0602), the National Natural Science Foundation of China (42305122), the Strategic Priority Research
435 Program of the Chinese Academy of Sciences (XDB40000000), and the Natural Science Basic Research Program
436 of Shaanxi (2023-JC-JQ-23). Qiyuan Wang also acknowledged the support from the Youth Innovation Promotion



437 Association of the Chinese Academy of Sciences.

438

439 **References**

440 Abas, M. R. B. and Simoneit, B. R.: Composition of extractable organic matter of air particles from Malaysia:
441 initial study, *Atmospheric Environment*, 30, 2779-2793, 1996.

442 Akindoyo, J. O., Beg, M., Ghazali, S., Islam, M., Jeyaratnam, N., and Yuvaraj, A.: Polyurethane types, synthesis
443 and applications—a review, *Rsc Advances*, 6, 114453-114482, 2016.

444 Arun, B. S., Gogoi, M. M., Hegde, P., Borgohain, A., Boreddy, S. K. R., Kundu, S. S., and Babu, S. S.:
445 Carbonaceous Aerosols over Lachung in the Eastern Himalayas: Primary Sources and Secondary Formation of
446 Organic Aerosols in a Remote High-Altitude Environment, *ACS Earth Space Chem.*, 5, 2493-2506,
447 10.1021/acsearthspacechem.1c00190, 2021.

448 Balducci, C., Perilli, M., Romagnoli, P., and Cecinato, A.: New developments on emerging organic pollutants in
449 the atmosphere, *Environmental Science and Pollution Research*, 19, 1875-1884, 10.1007/s11356-012-0815-2,
450 2012.

451 Barbaro, E., Zangrando, R., Moret, I., Barbante, C., Cescon, P., and Gambaro, A.: Free amino acids in atmospheric
452 particulate matter of Venice, Italy, *Atmospheric Environment*, 45, 5050-5057,
453 <https://doi.org/10.1016/j.atmosenv.2011.01.068>, 2011.

454 Barbaro, E., Zangrando, R., Vecchiato, M., Piazza, R., Cairns, W., Capodaglio, G., Barbante, C., and Gambaro,
455 A.: Free amino acids in Antarctic aerosol: potential markers for the evolution and fate of marine aerosol,
456 *Atmospheric Chemistry and Physics*, 15, 5457-5469, 2015.

457 Bian, Q., Alharbi, B., Shareef, M. M., Husain, T., Pasha, M. J., Atwood, S. A., and Kreidenweis, S. M.: Sources
458 of PM_{2.5} carbonaceous aerosol in Riyadh, Saudi Arabia, *Atmos. Chem. Phys.*, 18, 3969-3985, 10.5194/acp-18-
459 3969-2018, 2018.

460 Boreson, J., Dillner, A. M., and Peccia, J.: Correlating bioaerosol load with PM_{2.5} and PM₁₀cf concentrations: a
461 comparison between natural desert and urban-fringe aerosols, *Atmos. Environ.*, 38, 6029-6041,
462 <https://doi.org/10.1016/j.atmosenv.2004.06.040>, 2004.

463 Canonaco, F., Crippa, M., Slowik, J. G., Baltensperger, U., and Prévôt, A. S. H.: SoFi, an IGOR-based interface
464 for the efficient use of the generalized multilinear engine (ME-2) for the source apportionment: ME-2 application
465 to aerosol mass spectrometer data, *Atmos. Meas. Tech.*, 6, 3649-3661, 10.5194/amt-6-3649-2013, 2013.

466 Chen, Y., Cao, J. J., Zhao, J., Xu, H. M., Arimoto, R., Wang, G. H., Han, Y. M., Shen, Z. X., and Li, G. H.: n-
467 Alkanes and polycyclic aromatic hydrocarbons in total suspended particulates from the southeastern Tibetan
468 Plateau: Concentrations, seasonal variations, and sources, *SCIENCE OF THE TOTAL ENVIRONMENT*, 470, 9-
469 18, 10.1016/j.scitotenv.2013.09.033, 2014.

470 Cheng, Y., Li, S.-M., and Leithead, A.: Chemical Characteristics and Origins of Nitrogen-Containing Organic
471 Compounds in PM_{2.5} Aerosols in the Lower Fraser Valley, *Environmental Science & Technology*, 40, 5846-5852,
472 10.1021/es0603857, 2006.

473 Cohen, S. A. and Michaud, D. P.: Synthesis of a fluorescent derivatizing reagent, 6-aminoquinolyl-N-
474 hydroxysuccinimidyl carbamate, and its application for the analysis of hydrolysate amino acids via high-
475 performance liquid chromatography, *Anal Biochem*, 211, 279-287, 10.1006/abio.1993.1270, 1993.

476 Duo, B., Zhang, Y. C., Kong, L. D., Fu, H. B., Hu, Y. J., Chen, J. M., Li, L., and Qiong, A.: Individual particle
477 analysis of aerosols collected at Lhasa City in the Tibetan Plateau, *Journal of Environmental Sciences*, 29, 165-
478 177, 10.1016/j.jes.2014.07.032, 2015.



- 479 Ge, X., Wexler, A. S., and Clegg, S. L.: Atmospheric amines – Part I. A review, *Atmospheric Environment*, 45,
480 524-546, <https://doi.org/10.1016/j.atmosenv.2010.10.012>, 2011.
- 481 Golling, F. E., Pires, R., Hecking, A., Weikard, J., Richter, F., Danielmeier, K., and Dijkstra, D.: Polyurethanes for
482 coatings and adhesives—chemistry and applications, *Polymer International*, 68, 848-855, 2019.
- 483 Gonçalves, J. P. Z., Seraglio, J., Macuvele, D. L. P., Padoin, N., Soares, C., and Riella, H. G.: Green synthesis of
484 manganese based nanoparticles mediated by *Eucalyptus robusta* and *Corymbia citriodora* for agricultural
485 applications, *Colloids and Surfaces A: Physicochemical and Engineering Aspects*, 636, 128180,
486 <https://doi.org/10.1016/j.colsurfa.2021.128180>, 2022.
- 487 Gosselin, M. I., Rathnayake, C. M., Crawford, I., Pöhlker, C., Fröhlich-Nowoisky, J., Schmer, B., Després, V. R.,
488 Engling, G., Gallagher, M., and Stone, E.: Fluorescent bioaerosol particle, molecular tracer, and fungal spore
489 concentrations during dry and rainy periods in a semi-arid forest, *Atmospheric Chemistry and Physics*, 16, 15165-
490 15184, 2016.
- 491 Guo, H., Ding, A. J., So, K. L., Ayoko, G., Li, Y. S., and Hung, W. T.: Receptor modeling of source apportionment
492 of Hong Kong aerosols and the implication of urban and regional contribution, *Atmospheric Environment*, 43,
493 1159-1169, <https://doi.org/10.1016/j.atmosenv.2008.04.046>, 2009.
- 494 Han, B., Yang, W., Wang, J., Zhao, X. Y., Yin, B. H., Wang, X. H., Geng, C. M., Dou, X. Y., Xu, X., and Bai, Z.
495 P.: Characterizations and Potential Formation Pathways of Atmospheric Inorganic Ions at a National Background
496 Site in the Northeastern Qinghai-Tibet Plateau During Autumn Season, *Journal of Geophysical Research-
497 Atmospheres*, 125, 10.1029/2020jd032819, 2020.
- 498 Hejna, A., Barczewski, M., Kosmela, P., Mysiukiewicz, O., Tercjak, A., Piasecki, A., Saeb, M. R., and Szostak,
499 M.: Sustainable chemically modified poly (butylene adipate-co-terephthalate)/thermoplastic starch/poly (ϵ -
500 caprolactone)/cellulose biocomposites: looking at the bulk through the surface, *Journal of Materials Science*, 1-
501 21, 2024.
- 502 Ho, K. F., Ho, S. S. H., Huang, R.-J., Liu, S. X., Cao, J.-J., Zhang, T., Chuang, H.-C., Chan, C. S., Hu, D., and
503 Tian, L.: Characteristics of water-soluble organic nitrogen in fine particulate matter in the continental area of
504 China, *Atmospheric Environment*, 106, 252-261, <https://doi.org/10.1016/j.atmosenv.2015.02.010>, 2015.
- 505 Ho, S. S. H., Li, L., Qu, L., Cao, J., Lui, K. H., Niu, X., Lee, S.-C., and Ho, K. F.: Seasonal behavior of water-
506 soluble organic nitrogen in fine particulate matter (PM_{2.5}) at urban coastal environments in Hong Kong, *Air
507 Quality, Atmosphere & Health*, 12, 389-399, 10.1007/s11869-018-0654-5, 2019.
- 508 Hsu, C.-Y., Chiang, H.-C., Lin, S.-L., Chen, M.-J., Lin, T.-Y., and Chen, Y.-C.: Elemental characterization and
509 source apportionment of PM₁₀ and PM_{2.5} in the western coastal area of central Taiwan, *Science of The Total
510 Environment*, 541, 1139-1150, <https://doi.org/10.1016/j.scitotenv.2015.09.122>, 2016.
- 511 Lesage, J., DeGraff, I., and Danchik, R.: Isocyanates: Sampling, Analysis, and Health Effects, ASTM2001.
- 512 Li, M., Zhang, Q., Kurokawa, J. I., Woo, J. H., He, K., Lu, Z., Ohara, T., Song, Y., Streets, D. G., Carmichael, G.
513 R., Cheng, Y., Hong, C., Huo, H., Jiang, X., Kang, S., Liu, F., Su, H., and Zheng, B.: MIX: a mosaic Asian
514 anthropogenic emission inventory under the international collaboration framework of the MICS-Asia and HTAP,
515 *Atmos. Chem. Phys.*, 17, 935-963, 10.5194/acp-17-935-2017, 2017.
- 516 Li, W. J., Chen, S. R., Xu, Y. S., Guo, X. C., Sun, Y. L., Yang, X. Y., Wang, Z. F., Zhao, X. D., Chen, J. M., and
517 Wang, W. X.: Mixing state and sources of submicron regional background aerosols in the northern Qinghai-Tibet
518 Plateau and the influence of biomass burning, *Atmos. Chem. Phys.*, 15, 13365-13376, 10.5194/acp-15-13365-
519 2015, 2015.
- 520 Li, Y., Fu, T.-M., Yu, J. Z., Yu, X., Chen, Q., Miao, R., Zhou, Y., Zhang, A., Ye, J., Yang, X., Tao, S., Liu, H., and
521 Yao, W.: Dissecting the contributions of organic nitrogen aerosols to global atmospheric nitrogen deposition and
522 implications for ecosystems, *National Science Review*, 10, 10.1093/nsr/nwad244, 2023.



- 523 Lin, C., Huang, R.-J., Duan, J., Zhong, H., and Xu, W.: Primary and Secondary Organic Nitrate in Northwest
524 China: A Case Study, *Environ. Sci. Technol. Lett.*, 8, 947-953, 10.1021/acs.estlett.1c00692, 2021.
- 525 Lin, C., Huang, R.-J., Ceburnis, D., Buckley, P., Preissler, J., Wenger, J., Rinaldi, M., Facchini, M. C., O' Dowd,
526 C., and Ovadnevaite, J.: Extreme air pollution from residential solid fuel burning, *Nat. Sustain.*, 1, 512-517,
527 10.1038/s41893-018-0125-x, 2018.
- 528 Liu, H., Wang, Q., Xing, L., Zhang, Y., Zhang, T., Ran, W., and Cao, J.: Measurement report: quantifying source
529 contribution of fossil fuels and biomass-burning black carbon aerosol in the southeastern margin of the Tibetan
530 Plateau, *Atmos. Chem. Phys.*, 21, 973-987, 10.5194/acp-21-973-2021, 2021a.
- 531 Liu, H. K., Wang, Q. Y., Xing, L., Zhang, Y., Zhang, T., Ran, W. K., and Cao, J. J.: Measurement report:
532 quantifying source contribution of fossil fuels and biomass-burning black carbon aerosol in the southeastern
533 margin of the Tibetan Plateau, *Atmos. Chem. Phys.*, 21, 973-987, 10.5194/acp-21-973-2021, 2021b.
- 534 Meena, V. S., Maurya, B., and Verma, J. P.: Does a rhizospheric microorganism enhance K⁺ availability in
535 agricultural soils?, *Microbiological research*, 169, 337-347, 2014.
- 536 Meng, J. J., Wang, G. H., Li, J. J., Cheng, C. L., and Cao, J. J.: Atmospheric oxalic acid and related secondary
537 organic aerosols in Qinghai Lake, a continental background site in Tibet Plateau, *ATMOSPHERIC
538 ENVIRONMENT*, 79, 582-589, 10.1016/j.atmosenv.2013.07.024, 2013.
- 539 Murphy, B. N., Nolte, C. G., Sidi, F., Bash, J. O., Appel, K. W., Jang, C., Kang, D., Kelly, J., Mathur, R., Napelenok,
540 S., Pouliot, G., and Pye, H. O. T.: The Detailed Emissions Scaling, Isolation, and Diagnostic (DESID) module in
541 the Community Multiscale Air Quality (CMAQ) modeling system version 5.3.2, *Geosci. Model Dev.*, 14, 3407-
542 3420, 10.5194/gmd-14-3407-2021, 2021.
- 543 Nawrot, T. S., Alfaro-Moreno, E., and Nemery, B.: Update in occupational and environmental respiratory disease
544 2007, *American journal of respiratory and critical care medicine*, 177, 696-700, 2008.
- 545 Nielsen, C. J., Herrmann, H., and Weller, C.: Atmospheric chemistry and environmental impact of the use of
546 amines in carbon capture and storage (CCS), *Chemical Society Reviews*, 41, 6684-6704, 10.1039/C2CS35059A,
547 2012.
- 548 Petit, J. E., Favez, O., Albinet, A., and Canonaco, F.: A user-friendly tool for comprehensive evaluation of the
549 geographical origins of atmospheric pollution: Wind and trajectory analyses, *Environ. Modell. Softw.*, 88, 183-
550 187, 2017.
- 551 Priestley, M., Le Breton, M., Bannan, T. J., Leather, K. E., Bacak, A., Reyes-Villegas, E., De Vocht, F., Shallcross,
552 B. M. A., Brazier, T., Anwar Khan, M., Allan, J., Shallcross, D. E., Coe, H., and Percival, C. J.: Observations of
553 Isocyanate, Amide, Nitrate, and Nitro Compounds From an Anthropogenic Biomass Burning Event Using a ToF-
554 CIMS, *Journal of Geophysical Research: Atmospheres*, 123, 7687-7704, <https://doi.org/10.1002/2017JD027316>,
555 2018.
- 556 Qin, X., Wang, X., Shi, Y., Yu, G., Zhao, N., Lin, Y., Fu, Q., Wang, D., Xie, Z., Deng, C., and Huang, K.:
557 Characteristics of atmospheric mercury in a suburban area of east China: sources, formation mechanisms, and
558 regional transport, *Atmos. Chem. Phys.*, 19, 5923-5940, 10.5194/acp-19-5923-2019, 2019.
- 559 Ran, L., Deng, Z. Z., Wu, Y. F., Li, J. W., Bai, Z. X., Lu, Y., Zhuoga, D. Q., and Bian, J. C.: Measurement report:
560 Vertical profiling of particle size distributions over Lhasa, Tibet - tethered balloon-based in situ measurements
561 and source apportionment, *Atmos. Chem. Phys.*, 22, 6217-6229, 10.5194/acp-22-6217-2022, 2022.
- 562 Richardson, S. D. and Ternes, T. A.: Water Analysis: Emerging Contaminants and Current Issues, *Analytical
563 Chemistry*, 90, 398-428, 10.1021/acs.analchem.7b04577, 2018.
- 564 Salam, A., Hasan, M., Begum, B. A., Begum, M., and Biswas, S. K.: Chemical characterization of biomass burning
565 deposits from cooking stoves in Bangladesh, *Biomass and Bioenergy*, 52, 122-130,
566 <https://doi.org/10.1016/j.biombioe.2013.03.010>, 2013.



- 567 Salameh, D., Pey, J., Bozzetti, C., El Haddad, I., Detournay, A., Sylvestre, A., Canonaco, F., Armengaud, A., Piga,
568 D., Robin, D., Prevot, A. S. H., Jaffrezo, J. L., Wortham, H., and Marchand, N.: Sources of PM_{2.5} at an urban-
569 industrial Mediterranean city, Marseille (France): Application of the ME-2 solver to inorganic and organic markers,
570 Atmospheric Research, 214, 263-274, <https://doi.org/10.1016/j.atmosres.2018.08.005>, 2018.
- 571 Shi, J., Gao, H., Qi, J., Zhang, J., and Yao, X.: Sources, compositions, and distributions of water - soluble organic
572 nitrogen in aerosols over the China Sea, Journal of Geophysical Research: Atmospheres, 115, 2010.
- 573 Simoneit, B. R. T., Rushdi, A. I., bin Abas, M. R., and Didyk, B. M.: Alkyl Amides and Nitriles as Novel Tracers
574 for Biomass Burning, Environmental Science & Technology, 37, 16-21, 10.1021/es020811y, 2003.
- 575 Song, T., Wang, S., Zhang, Y., Song, J., Liu, F., Fu, P., Shiraiwa, M., Xie, Z., Yue, D., Zhong, L., Zheng, J., and
576 Lai, S.: Proteins and Amino Acids in Fine Particulate Matter in Rural Guangzhou, Southern China: Seasonal
577 Cycles, Sources, and Atmospheric Processes, Environmental Science & Technology, 51, 6773-6781,
578 10.1021/acs.est.7b00987, 2017.
- 579 Sorooshian, A., Murphy, S. M., Hersey, S., Gates, H., Padro, L. T., Nenes, A., Brechtel, F. J., Jonsson, H., Flagan,
580 R. C., and Seinfeld, J. H.: Comprehensive airborne characterization of aerosol from a major bovine source, Atmos.
581 Chem. Phys., 8, 5489-5520, 10.5194/acp-8-5489-2008, 2008.
- 582 Tan, T., Hu, M., Du, Z., Zhao, G., Shang, D., Zheng, J., Qin, Y., Li, M., Wu, Y., Zeng, L., Guo, S., and Wu, Z.:
583 Measurement report: Strong light absorption induced by aged biomass burning black carbon over the southeastern
584 Tibetan Plateau in pre-monsoon season, Atmos. Chem. Phys., 21, 8499-8510, 10.5194/acp-21-8499-2021, 2021.
- 585 Trapp, S. and Eggen, T.: Simulation of the plant uptake of organophosphates and other emerging pollutants for
586 greenhouse experiments and field conditions, Environmental Science and Pollution Research, 20, 4018-4029,
587 10.1007/s11356-012-1337-7, 2013.
- 588 Wang, M., Wang, Q., Ho, S. S. H., Li, H., Zhang, R., Ran, W., Qu, L., Lee, S.-c., and Cao, J.: Chemical
589 characteristics and sources of nitrogen-containing organic compounds at a regional site in the North China Plain
590 during the transition period of autumn and winter, Science of The Total Environment, 812, 151451,
591 <https://doi.org/10.1016/j.scitotenv.2021.151451>, 2022.
- 592 Wang, Q., Han, Y., Ye, J., Liu, S., Pongpiachan, S., Zhang, N., Han, Y., Tian, J., Wu, C., Long, X., Zhang, Q.,
593 Zhang, W., Zhao, Z., and Cao, J.: High Contribution of Secondary Brown Carbon to Aerosol Light Absorption in
594 the Southeastern Margin of Tibetan Plateau, Geophys. Res. Lett., 46, 4962-4970, 10.1029/2019gl082731, 2019a.
- 595 Wang, Q., Huang, X. H. H., Tam, F. C. V., Zhang, X., Liu, K. M., Yeung, C., Feng, Y., Cheng, Y. Y., Wong, Y. K.,
596 Ng, W. M., Wu, C., Zhang, Q., Zhang, T., Lau, N. T., Yuan, Z., Lau, A. K. H., and Yu, J. Z.: Source apportionment
597 of fine particulate matter in Macao, China with and without organic tracers: A comparative study using positive
598 matrix factorization, Atmospheric Environment, 198, 183-193, <https://doi.org/10.1016/j.atmosenv.2018.10.057>,
599 2019b.
- 600 Wang, Q. Q., Huang, X. H., Zhang, T., Zhang, Q., Feng, Y., Yuan, Z., Wu, D., Lau, A. K., and Yu, J. Z.: Organic
601 tracer-based source analysis of PM_{2.5} organic and elemental carbon: A case study at Dongguan in the Pearl River
602 Delta, China, Atmospheric Environment, 118, 164-175, 2015.
- 603 Wang, X., Shen, Z., Liu, F., Lu, D., Tao, J., Lei, Y., Zhang, Q., Zeng, Y., Xu, H., Wu, Y., Zhang, R., and Cao, J.:
604 Saccharides in summer and winter PM_{2.5} over Xi'an, Northwestern China: Sources, and yearly variations of
605 biomass burning contribution to PM_{2.5}, Atmospheric Research, 214, 410-417,
606 <https://doi.org/10.1016/j.atmosres.2018.08.024>, 2018.
- 607 Wu, C. and Yu, J. Z.: Determination of primary combustion source organic carbon-to-elemental carbon (OC/EC)
608 ratio using ambient OC and EC measurements: secondary OC-EC correlation minimization method, Atmos. Chem.
609 Phys., 16, 5453-5465, 10.5194/acp-16-5453-2016, 2016.
- 610 Yu, X., Li, Q., Liao, K., Li, Y., Wang, X., Zhou, Y., Liang, Y., and Yu, J. Z.: New measurements reveal a large



611 contribution of nitrogenous molecules to ambient organic aerosol, *npj Clim. Atmos. Sci.*, 7, 72, 10.1038/s41612-
612 024-00620-6, 2024.

613 Yuan, G. L., Wu, M. Z., Sun, Y., Li, J., Li, J. C., and Wang, G. H.: One century of air deposition of hydrocarbons
614 recorded in travertine in North Tibetan Plateau, China: Sources and evolution, *Sci. Total Environ.*, 560, 212-217,
615 10.1016/j.scitotenv.2016.03.227, 2016.

616 Zhang, N. N., Cao, J. J., Wang, Q. Y., Huang, R. J., Zhu, C. S., Xiao, S., and Wang, L. L.: Biomass burning
617 influences determination based on PM_{2.5} chemical composition combined with fire counts at southeastern Tibetan
618 Plateau during pre-monsoon period, *ATMOSPHERIC RESEARCH*, 206, 108-116,
619 10.1016/j.atmosres.2018.02.018, 2018.

620 Zhang, Q. and Anastasio, C.: Free and combined amino compounds in atmospheric fine particles (PM_{2.5}) and fog
621 waters from Northern California, *Atmospheric Environment*, 37, 2247-2258, [https://doi.org/10.1016/S1352-](https://doi.org/10.1016/S1352-2310(03)00127-4)
622 [2310\(03\)00127-4](https://doi.org/10.1016/S1352-2310(03)00127-4), 2003a.

623 Zhang, Q. and Anastasio, C.: Free and combined amino compounds in atmospheric fine particles (PM_{2.5}) and
624 fog waters from Northern California, *Atmospheric Environment*, 37, 2247-2258, 2003b.

625 Zhang, X. H., Xu, J. Z., and Kang, S. C.: Chemical characterization of submicron particulate matter
626 (PM_₁) emitted by burning highland barley in the northeastern part of the Qinghai-Tibet Plateau,
627 *Atmos. Environ.*, 224, 10.1016/j.atmosenv.2020.117351, 2020.

628 Zhang, X. H., Xu, J. Z., Kang, S. C., Zhang, Q., and Sun, J. Y.: Chemical characterization and sources of submicron
629 aerosols in the northeastern Qinghai-Tibet Plateau: insights from high-resolution mass spectrometry, *Atmos.*
630 *Chem. Phys.*, 19, 7897-7911, 10.5194/acp-19-7897-2019, 2019.

631 Zhao, W. H., Zhang, X. H., Zhai, L. X., Shen, X. J., and Xu, J. Z.: Chemical characterization and sources of
632 submicron aerosols in Lhasa on the Qinghai-Tibet Plateau: Insights from high-resolution mass spectrometry, *Sci.*
633 *Total Environ.*, 815, 10.1016/j.scitotenv.2021.152866, 2022.

634 Zhao, Z. Z., Cao, J. J., Shen, Z. X., Huang, R. J., Hu, T. F., Wang, P., Zhang, T., and Liu, S. X.: Chemical
635 composition of PM_{2.5} at a high-altitude regional background site over Northeast of Tibet Plateau,
636 *ATMOSPHERIC POLLUTION RESEARCH*, 6, 815-823, 10.5094/APR.2015.090, 2015.

637 Zhao, Z. Z., Wang, Q. Y., Li, L., Han, Y. M., Ye, Z. L., Pongpiachan, S., Zhang, Y., Liu, S. X., Tian, R. X., and
638 Cao, J. J.: Characteristics of PM_{2.5} at a High-Altitude Remote Site in the Southeastern Margin of the Tibetan
639 Plateau in Premonsoon Season, *Atmosphere*, 10, 10.3390/atmos10110645, 2019.

640 Zhu, R.-g., Xiao, H.-Y., Zhu, Y., Wen, Z., Fang, X., and Pan, Y.: Sources and Transformation Processes of
641 Proteinaceous Matter and Free Amino Acids in PM_{2.5}, *J. Geophys. Res. Atmos.*, 125, e2020JD032375,
642 <https://doi.org/10.1029/2020JD032375>, 2020.

643



644 **Table 1** Concentration levels of chemical compounds and groups in Gaomeigu, China. (ng m⁻³).

Species	Mean	SD ^a	Min ^b	Max ^c
NOCs (ng m⁻³)				
Major Compound Classes				
FAAs				
Protein FAAs	989.5	403.5	337.8	1857.5
Non-protein FAAs	103.3	41.8	32.5	206.8
Total FAAs	1092.9	443.4	370.2	2033.2
Amines				
Aliphatic Amines	508.9	225.9	158.5	1032.2
Aromatic Amines	2.6	1.0	1.0	5.3
Other Amines	51.8	16.8	29.2	100.7
Total Amines	563.3	240.2	190.2	1113.5
Urea	266.4	119.0	79.4	588.8
Total Major Compound	1922.6	790.5	649.0	3543.7
Minor Compound Classes				
Amides				
Alkyl amides (Odd)	13.1	5.8	4.1	26.6
Alkyl amides (Even)	21.4	8.9	6.6	41.2
Total Alkyl amides	45.1	18.6	14.9	84.6
Nitriles				
Alkyl nitriles (Odd)	1.9	0.7	0.8	3.5
Alkyl nitriles (Even)	2.7	1.0	1.0	4.8
Total Alkyl nitriles	4.7	1.7	1.8	8.2
Cyclic NOCs	136.2	61.6	42.1	291.9
Isocyanates	10.9	4.7	3.3	23.2
Total Minor Compound	196.8	86.1	65.4	404.4
Total NOCs	2119.4	875.0	714.4	3887.1

645 ^aSD represents standard deviation. ^bMin and ^cMax denote “minimum and maximum, respectively.

646



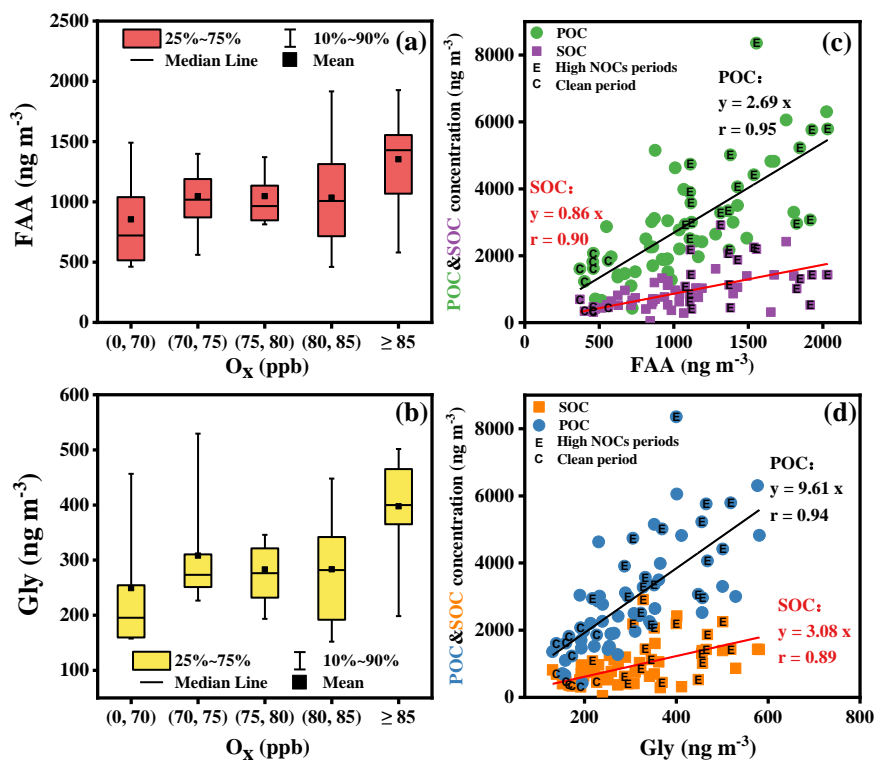
647

648 **Figure 1** Hourly variations in meteorological parameters and daily chemical compositions of NOCs during
649 different events in Gaomeigu in 2018 (EP1: 3/22 to 3/26; EP2: 3/30 to 4/6; EP3: 4/17 to 4/18; EP4: 4/25
650 to 4/28; Clean period: 5/6 to -5/11).

651



652



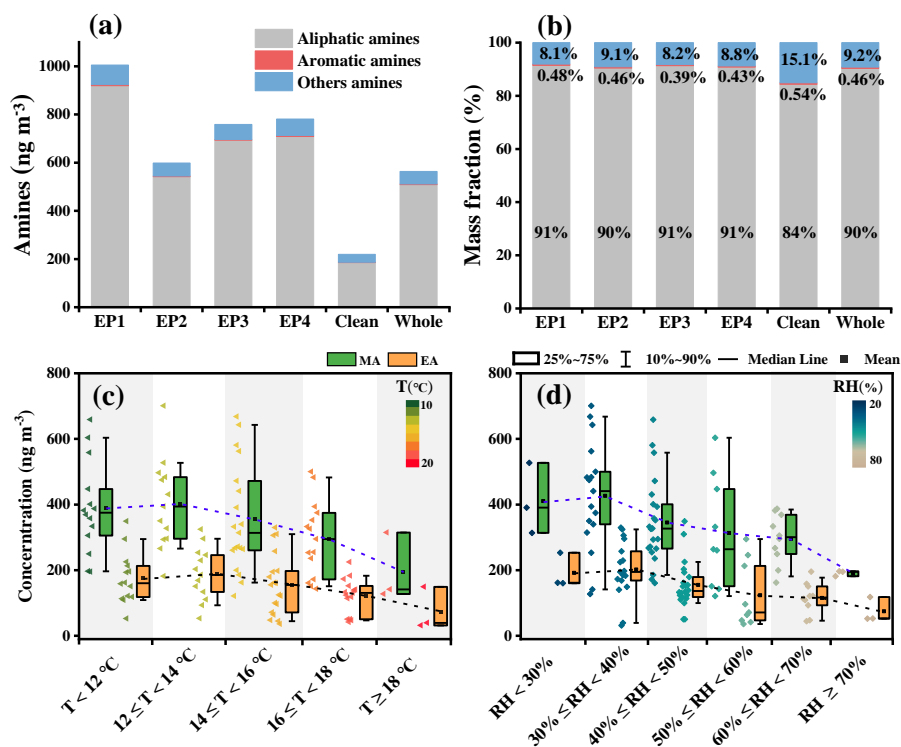
653 **Figure 2** (a) FAA dependence of O₃; (b) Gly dependence of O₃; Correlation plots of POC&SOC
 654 concentration versus (c) FAA, and (d) Gly. The box represents the 25th (bottom) and 75th percentiles (top),
 655 and the box-whisker data represent the range from 10th to 90th percentiles.

656



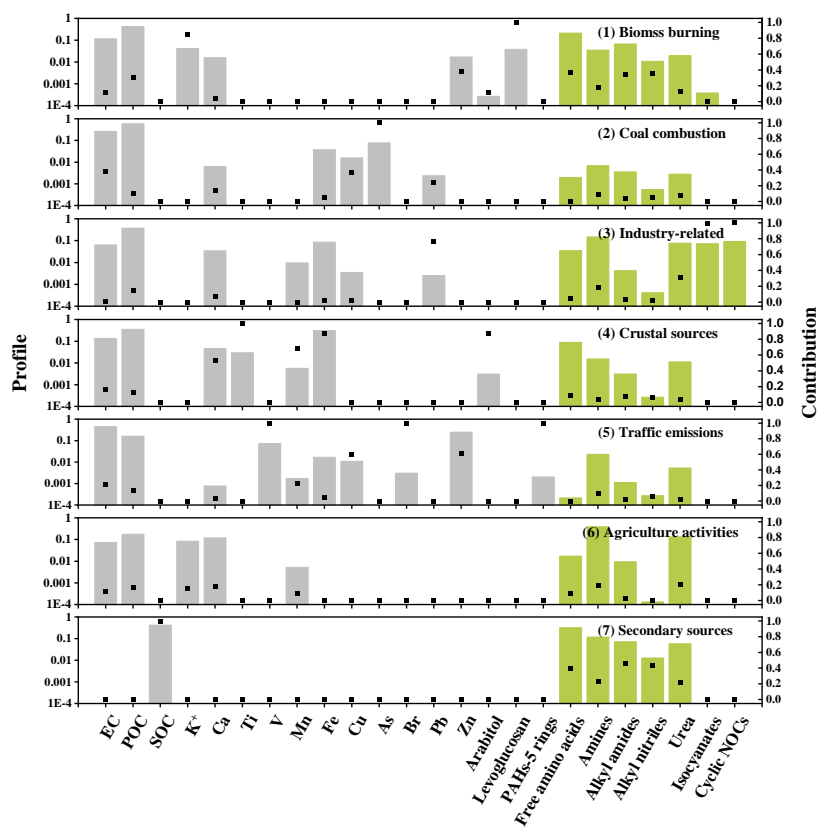
657

658



659 **Figure 3** (a) Concentration and (b) composition of amines. (c) Temperature dependence of EA and MA,
 660 and (d) RH dependence of EA and MA. The box represents the 25th (bottom) and 75th percentiles (top),
 661 and the box-whisker data represents the 10th to 90th percentiles.

662



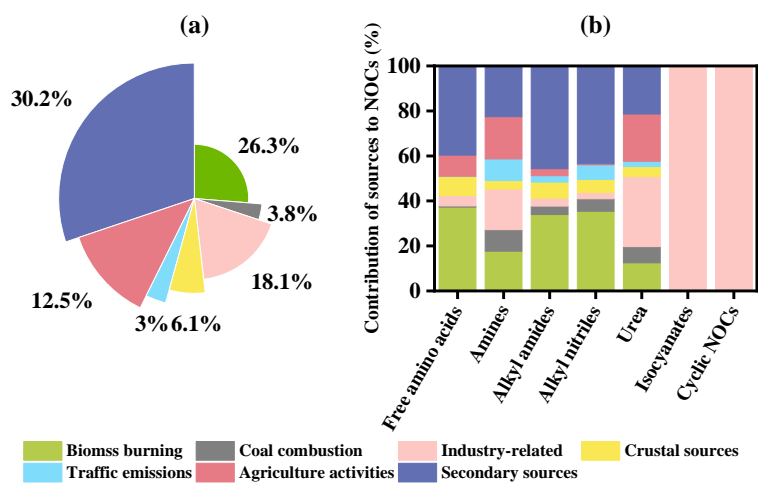
663

664 **Figure 4** The factor profiles and explained variations in the ME-2 modeling.

665



666



667

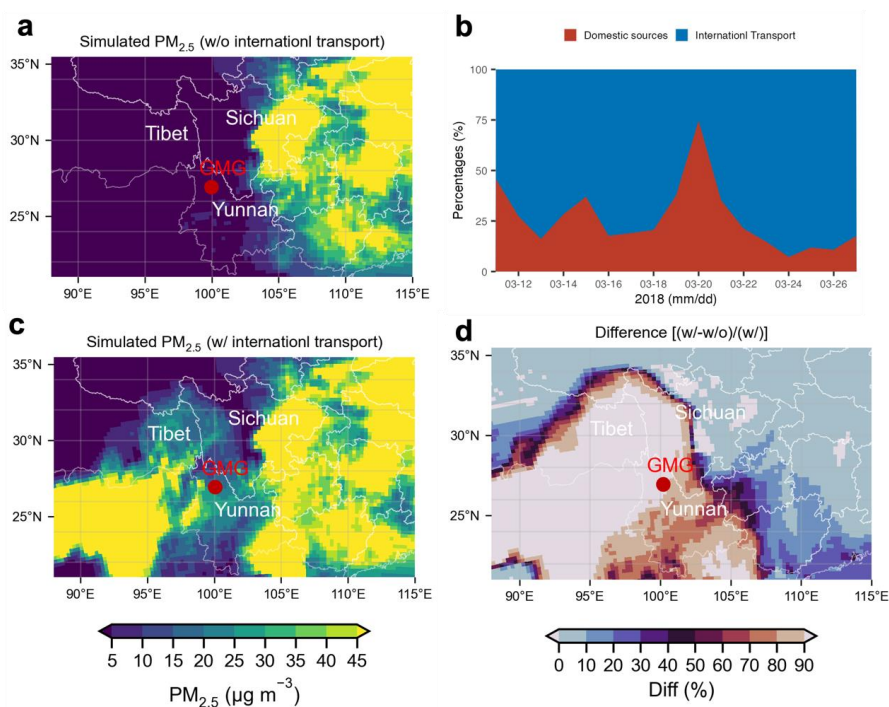
668

Figure 5 Contributions of each source to (a) total NOCs; and (b) seven classes NOC species.

669



670



671

672 **Figure 6.** (a) Distribution of PM_{2.5} concentrations resulting solely from China's domestic emissions

673 (MEIC-China only); (b) Proportionate contributions of domestic versus international PM_{2.5} transport

674 during the simulation window of March 11th -27th 2018; (c) Distribution of PM_{2.5} incorporating both

675 domestic and international transport influences (MEIC-China+MIX); (d) Difference of contribution of

676 international transport to PM_{2.5} concentrations, derived from the differential analysis [(c)-(a)]/(c).

677